

Composition of the solar atmosphere

A. Mohan and B. N. Dwivedi*

Department of Applied Physics, Institute of Technology, Banaras Hindu University, Varanasi 221 005, India

Unlike the uniform composition of the Sun's photosphere, the composition of the Sun's atmosphere is not well defined. Systematic differences do exist between the composition of the solar corona and the photosphere. Spatial and time variability in the composition of various coronal features have also been reported. We review the spectroscopic techniques used and the progress made in recent years to derive the plasma compositions of various structures in the solar atmosphere.

THE knowledge of chemical composition of cosmic as well as laboratory plasmas is of universal importance. The plasma composition plays a key role in our understanding of physical processes that transport, accelerate and heat the plasmas and the wind. It must also be known to interpret the spectral signature, density, temperature, emission measures, radiation losses, etc. of the plasmas. In 1929, Russell¹, whose name is associated with pioneering researches in astrophysics (e.g. H-R diagram) and in atomic spectroscopy (e.g. LS or Russell-Saunders coupling), made the first quantitative analysis of the chemical composition of the solar atmosphere. Using eye estimates of the solar line intensities, he derived the abundances of 56 elements. Russell also showed that the solar atmosphere and, finally, the universe were essentially made of hydrogen. Many of the remarkable features correlated to nuclear properties² (Figure 1), giving clues to the origin of the different elements, were already present in Russell's results. Twenty years later in 1948, using better observations and better techniques, Unsöld³ obtained abundance results for 25 elements, while noting that his results were not much different from Russell's values. He concluded that this was not surprising because Russell had an 'unvergleichliches spektroskopisches Fingerspitzengefühl' (an incomparable spectroscopic flair).

Chemical-composition data concerning the solar outer layers above the photosphere slowly accumulated during the last three decades. The data, obtained from the ground and from space, revealed a great variability from one layer to another, and from one event to another. Despite these variabilities and sometimes large differences with photospheric results, the data play an important role in defining the solar chemical composition and, more importantly, in explaining the physical processes that allow

these outermost layers to exist. Solar abundance results are generally compared with the accurate results obtained from a rare class of meteorites, the CI carbonaceous chondrites. As can be seen from Figure 2, photospheric and meteoritic results now agree perfectly well^{4,5}. The fifteen most abundant elements in the solar photosphere that are relevant to solar and stellar atmospheres are given in Table 1. Values are given in the usual logarithmic (dex) scale, $A_{\text{el}} = \log N_{\text{el}}/N_{\text{H}} + 12.0$, where N_{el} is the abundance by number.

Early indications of anomalous coronal composition were seen in low-speed solar wind and energetic particle data⁶⁻⁸. Elements with first ionization potential (FIP) ≤ 10 eV were found to be overabundant by about a factor of 4 relative to elements with FIP ≥ 10 eV compared to the photosphere. This suggested that a separation of ions from neutrals at the base of the atmosphere could be responsible. Direct spectroscopic evidence for a systematic abundance difference between the corona and the photosphere was also found in solar ultraviolet spectra^{9,10}. The elements Mg, Al, and Si were found to be three times more abundant in the outer solar atmosphere compared to the then standard photospheric abundances¹¹. Meyer¹² updated the review of the ultraviolet spectroscopic abundances and drew upon the extensive data on solar wind and solar energetic particles abundances to better define the basic composition difference between the photosphere and the outer solar atmosphere. All abundances showed the same basic pattern of an under-abundance of the heavy elements with FIP > 10 eV (high-FIP) relative to elements with FIP < 10 eV (low-FIP) by a factor of 4 to 6 compared to standard local galactic or solar photospheric composition. This correlation of the solar coronal compo-

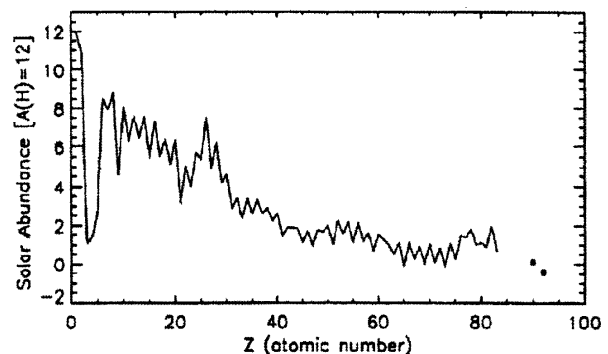


Figure 1. Distribution of element abundances as a function of atomic number².

*For correspondence. (e-mail: dwivedi@bhu.ac.in)

sition with FIP further suggested an ion–neutral separation during the rise of the matter from the underlying chromosphere, which is cool enough to contain neutrals. A schematic representation of the change in the solar atmosphere elemental abundances relative to the photosphere versus the FIP, known as FIP effect, is shown¹³ in Figure 3.

Spectroscopic diagnostics for elemental abundances

Line intensities

Following Seaton¹⁴, the collisional excitation rate per unit volume between initial level *i* and upper level *u* of line emission is given by

$$N_i a_{iu} N_e = 8.63 \times 10^{-6} N_i \frac{\Omega_{iu}}{w_i} \frac{e^{-\Delta E_{iu}/kT}}{T^{1/2}} N_e \text{ cm}^{-3} \text{ s}^{-1}. \quad (1)$$

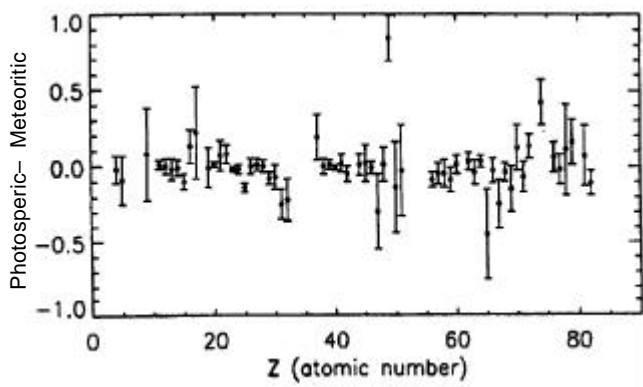


Figure 2. Difference between solar and meteoritic abundances of elements as a function of atomic number⁴. Error bars represent the uncertainty of the solar abundance determinations.

Here N_i is the number density of the initial level *i*, N_e is the electron density, Ω_{iu} is the collision strength, and w_i is the statistical weight of the initial level. The volume emission coefficient in a radiative transition from the upper level *u* to a lower level *l* is then given by

$$e(I_{ul}) = \frac{1}{4\pi} \frac{hc}{I} \frac{A_{ul}}{\sum_l A_{ul}} \sum_i N_i a_{iu} N_e \text{ ergs cm}^{-3} \text{ s}^{-1} \text{ sr}^{-1}, \quad (2)$$

where we have summed over all initial levels of the emitting ion, which make a contribution to the population of the upper state. From eqs (1) and (2) we have

$$e(I_{ul}) = \frac{1.36 \times 10^{-22}}{I(\text{cm})} \left(N_g \frac{\Omega_{gu}}{w_g} + N_1 \frac{\Omega_{1u}}{w_1} + N_2 \frac{\Omega_{2u}}{w_2} + \dots \right) \times \frac{A_{ul}}{\sum_l A_{ul}} \frac{e^{-\Delta E/kT}}{T^{1/2}} N_e \text{ ergs cm}^{-3} \text{ s}^{-1} \text{ sr}^{-1}. \quad (3)$$

Here N_g represents the number density in the ground state and assuming that the other contributing levels are sufficiently close to the ground level, we take a mean value for the energy difference $\Delta E \approx E_u - E_i$.

We rewrite the expression in parentheses as

$$\left[\frac{\Omega_{iu}}{w_i} \right] = \frac{\Omega_{gu}}{w_g} + \frac{N_1}{N_g} \frac{\Omega_{1u}}{w_1} + \frac{N_2}{N_g} \frac{\Omega_{2u}}{w_2} + \dots \quad (4)$$

The number density in the ground level is rewritten as

$$N_g = \frac{N_g}{N(X^{+m})} \frac{N(X^{+m})}{N(X)} \frac{N(X)}{N(\text{H})} \frac{N(\text{H})}{N_e} N_e. \quad (5)$$

Table 1. First ionization potential, photospheric and solar atmosphere abundances above quiet regions⁴

Element	Ionization potential (eV)	Photospheric abundance		
		Log ₁₀	Log ₁₀ solar abundance above typical quiet regions	
			$3 \times 10^4 \leq T \leq 8 \times 10^5 \text{ K}$	$\sim 1.4 \times 10^6 \text{ K}$
1 H	13.6	12.00	12.00	12.00
2 He	24.6	10.93	10.93	10.93
6 C	11.3	8.52	8.52	8.52
7 N	14.5	7.92	7.92	7.92
8 O	13.6	8.83	8.83	8.83
10 Ne	21.6	8.11	8.11	8.11
11 Na	5.1	6.32	6.62	6.92
12 Mg	7.6	7.58	7.88	8.18
13 Al	6.0	6.49	6.79	7.09
14 Si	8.2	7.56	7.86	8.16
16 S	10.4	7.33	7.33	7.33
18 Ar	15.8	6.59	6.59	6.59
20 Ca	6.1	6.35	6.65	6.95
26 Fe	7.9	7.50	7.80	8.10
28 Ni	7.6	6.25	6.55	6.85

Here $N(X^{+m})/N(X)$ is the relative ion population at temperature T , and $N(X)/N(H)$ is the elemental abundance relative to hydrogen. We also write

$$N(X^{+m}) = N_g \left(1 + \frac{N_1}{N_g} + \frac{N_2}{N_g} + \dots \right). \quad (6)$$

For a fully ionized plasma with a 10% helium abundance $N(H)/N_e = 0.83$. Adopting this value and substituting eqs (4)–(6) in eq. (3), we get the total line intensity emitted in a transition from upper level u to lower level l by a cm^2 plasma column on the Sun along the line of sight from Earth¹⁵:

$$I(I_{ul}) = \frac{1.13 \times 10^{-22} \left[\frac{\Omega_{iu}}{w_i} \right] \times \frac{1}{1 + \sum_i N_i/N_g} \frac{A_{ul}}{\sum_l A_{ul}} \frac{N(X)}{N(H)} \int G(T) N_e^2 ds, \quad (7)$$

where

$$G(T) = \frac{N(X^{+m})}{N(X)} \frac{e^{-\tilde{A}E/kT}}{T^{1/2}}. \quad (8)$$

The ionization fraction $N(X^{+m})/N(X)$ is adopted^{16,17}. The averaged value of $G(T)$ is estimated to a constant logarithmic width of $\Delta \log T = \log T_{\max} \pm 0.15$, which corresponds to temperature limits of $1.412 T_{\max}$ and $0.708 T_{\max}$, so that

$$\langle G(T) \rangle = G(T) dT / 0.704 T_{\max} = b G_{\max}, \quad (9)$$

where G_{\max} is the maximum value of $G(T)$ and b is the normalizing constant.

Adopting eq. (9) for the average value of $G(T)$ and removing it from the integral in eq (7), we get the final expression

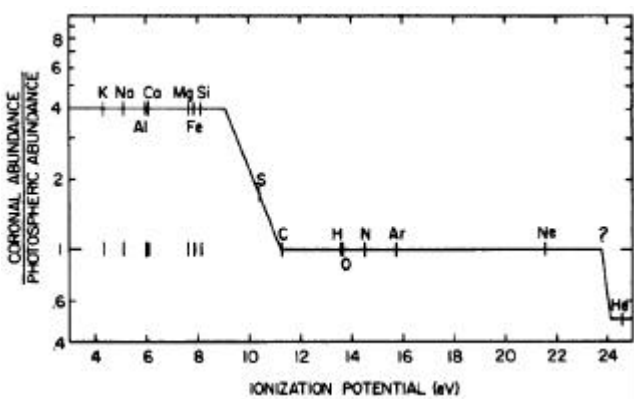


Figure 3. FIP effect observed in coronal abundances. Elements with first ionization potential (FIP) < 10 eV are four times more abundant in the corona than elements with FIP > 10 eV compared to the photosphere¹³.

$$I(I_{ul}) = \frac{1.13 \times 10^{-22} \left[\frac{\Omega_{iu}}{w_i} \right] \times \frac{1}{1 + \sum_i N_i/N_g} \frac{A_{ul}}{\sum_l A_{ul}} b G_{\max} \frac{N(X)}{N(H)} \times \int N_e^2 \frac{ds}{dT} dT. \quad (10)$$

Another approach to the problem of different temperature widths is to remove an average value of $\int N_e^2 ds / dT$ from the integral in eq (10) to obtain the intensity equation in the form

$$I(I_{ul}) = \frac{1.13 \times 10^{-22} \left[\frac{\Omega_{iu}}{w_i} \right] \times \frac{1}{1 + \sum_i N_i/N_g} \frac{A_{ul}}{\sum_l A_{ul}} \frac{N(X)}{N(H)} \times \left\langle N_e^2 \frac{ds}{dT} \right\rangle \int G(T) dT. \quad (11)$$

A plot of the resulting values of

$$\left\langle N_e^2 \frac{ds}{dT} \right\rangle \text{ vs } T_{\max}$$

for the various ions should be more nearly consistent with each other than the values of $\int N_e^2 ds$. The empirical plot of

$$\left\langle N_e^2 \frac{ds}{dT} \right\rangle \text{ vs } T_{\max}$$

can be adjusted by iteration until the observed line intensities are reproduced.

Line ratios

Composition studies using observations from the SUMER (Solar Ultraviolet Measurements of Emitted Radiation) and CDS (Coronal Diagnostic Spectrometer) spectrometers on the SOHO (Solar and Heliospheric Observatory) spacecraft have tended to use the line-ratio method to determine anomalous element abundance ratios and thereby the FIP bias factor in various coronal plasmas. In cases where two ions of different elements peak at the same T_{\max} and show a nearly identical $G(T)$ function, the values of

$$\left\langle N_e^2 \frac{ds}{dT} \right\rangle$$

for the two ions will be nearly the same and cancel from the equation when the ratio of two line intensities is considered. This is a convenient way to derive an abundance ratio from the ratio of two observed line intensities.

In order to obtain the relative abundances of two elements X and Y , ratios of spectral line intensities from the two elements are used. The line intensity ratio R of two lines is given by

$$R = \frac{\ddot{e}_{k\ell} A_{ji} N_j(X^{+m})/N(X^{+m})}{\ddot{e}_{ij} A_{\ell k} N_\ell(Y^{+m})/N(Y^{+m})} \times \frac{N(X^{+m})/N(X)}{N(Y^{+m})/N(Y)} \cdot \frac{N(X)}{N(Y)} \quad (12)$$

As already noted, if the intensities of the two lines have a similar temperature dependence, then the lines are presumably formed in the same plasma volume and at the same density. For determining the relative element abundance between X and Y , we can then compute a theoretical line-intensity ratio assuming equal abundances for X and Y , and subsequently deduce $N(X)/N(Y)$ from the observed line-intensity ratio R_{obs} . Theoretical line ratios are computed using the CHIANTI database^{18,19} and the density and temperature values are deduced from the observations, assuming unity elemental abundances.

Abundances of the noble gases

The first three noble gases in the periodic table of elements, namely helium, neon and argon have ionization potentials of 24.6, 21.6 and 15.8 eV respectively. Due to the correspondingly high energies of their first excited levels, no absorption lines from He I, Ne I and Ar I have been observed in the photospheric spectrum. As a result, their photospheric abundances have never been established by a direct measurement. In the case of He, the task is much more difficult because the only existing He species besides the neutral one is He^+ . And the energy of its first excited level is at $E = 40$ eV, a much higher value when compared with the temperature of maximum fractional abundance of the ion ($kT \sim 8$ eV). The excitation rate (C_{gu}) of the first excited He^+ level is temperature-dependent:

$$C_{gu} \propto T^{-1/2} e^{-\ddot{A}E/kT} \propto T_e^{-1/2} e^{-5}.$$

The Boltzmann factor being sensitive to temperature variations, relatively small changes in temperature result in large changes in the level excitation, and thereby in the line intensity. In the absence of any independent way to determine the plasma temperature, observed intensity changes could easily be interpreted as due either to temperature or abundance, making He abundance determination in the so-called transition region complex.

Neon and argon do not have absorption lines in the solar photospheric spectrum. Therefore, for a long time the solar abundances of these elements have been assumed to be similar to ‘local galactic values’ derived from H II regions,

nebulae and hot stars. The dispersed spectroheliograph images of the flare in the 300–600 Å region showed a bright Doppler-widened impulsive emission streak which was the feature traced and calibrated for intensities. Several density-sensitive line ratios yielded an electron density of $2\text{--}3 \times 10^{12} \text{ cm}^{-3}$, consistent with the assumed low-altitude source region of the flare. The analysis of the image intensities for relative abundances was then carried out. From the overlap of the neon ions with the magnesium ions, a Ne/Mg abundance ratio of 3.6 was determined. Similarly, the Ar/Mg ratio of 0.15 was determined. This was later corrected to 0.11 by use of improved collision strengths for levels in the Ar^{+6} ion. The O/Mg ratio determined by similar methods was 24 ± 4 . This compared with the photospheric value of 21.7 and thus confirmed the photospheric source region of the flare. As the last step, the abundance ratios were converted to absolute values using the well-determined photospheric abundance of magnesium⁴: $\log \text{Mg} = 7.58 \pm 0.05$, $\log \text{neon} = 8.13 \pm 0.10$, $\log \text{argon} = 6.62 \pm 0.12$.

He abundance

The He^+ ion is most abundant at a transition-region temperature of ~ 8 eV. At coronal temperatures of ~ 100 eV and higher, the fractional abundance of He^+ becomes small, and the Boltzmann factor ($\sim e^{-40/100}$) becomes quite insensitive to temperature changes. Despite the low fractional abundance of He^+ , He II lines emitted by coronal plasmas could be reliably detected. Gabriel *et al.*²⁰ made the first direct attempt to determine the He abundance in the solar corona using data from the CHASE experiment on-board the NASA Spacelab II mission. The intensity ratio between the 1216 Å H I resonance line and the 304 Å He II resonance line yielded a He/H abundance of 0.070 ± 0.011 . Feldman²¹ used the intensity ratio between the 1085 Å He II Bag line and the 1031 Å O VI resonance line recorded by SUMER from a quiet coronal equatorial region to derive the He abundance. The two lines were selected not only because of their relative strength and close wavelength proximity, but also because at coronal temperatures their intensity ratio is calculated to be fairly insensitive to temperature variations. Using the best available theoretical emissivity calculations and the measured intensities, a He/H abundance value of 0.085 ± 0.015 was derived. The estimated 15% uncertainty was attributed mostly to uncertainties in the theoretical atomic cross-sections. Recently, Laming and Feldman²² repeated the He abundance measurement using improved atomic data and a modified oxygen photospheric abundance value. This gave the He/H abundance of $0.052 \pm 10\%$, where the uncertainty is dominated by the counting statistics, the subtraction of the scattered light and the atomic data. This value of He abundance is similar to He abundance values measured in the slow-speed solar wind. As a result, there may not be a real depletion of helium in the slow solar wind as as-

sumed by many investigators, who have adopted significantly larger He/H ratios in the photosphere.

FIP bias in solar structures

The evidence for a systematic difference between coronal and photospheric abundances¹² renewed the interest in solar abundances, especially in the FIP bias in different solar structures (Figure 4). The unexplained variability of the Ne VI lines at 400 Å relative to the adjacent lines of Mg VI noted in Skylab spectroheliograms was presented by Sheeley²³. The most interesting result¹² is the typical O/Mg ratio obtained from the corona to be approximately 6. However, this ratio is 17.8 in the erupting prominence, which is similar to the well-documented photospheric ratio of 21.7, thereby indicating that essentially photospheric plasma was entrained and ejected in the magnetic field of the erupting prominence. The neon abundance had not previously been measured in photospheric plasmas. Estimates of the Ne/Mg photospheric ratio based on measurements in H II regions and hot stars suggested a value of about 3.1. Measurements of this ratio in the corona were always less than 1, reflecting the FIP bias factor.

The best Skylab example for measuring photospheric abundances was, however, one in which the photospheric material was heated in place to flare temperatures. This was the impulsive flare of 2 December 1973 which enabled the photospheric abundances of neon and argon to be directly measured for the first time. Here we may just recall that the O/Mg ratio of 24 determined from the emission lines was in good agreement with the photospheric ratio of 21.7 from absorption lines and confirmed that the plasma source of the flare was indeed photo-

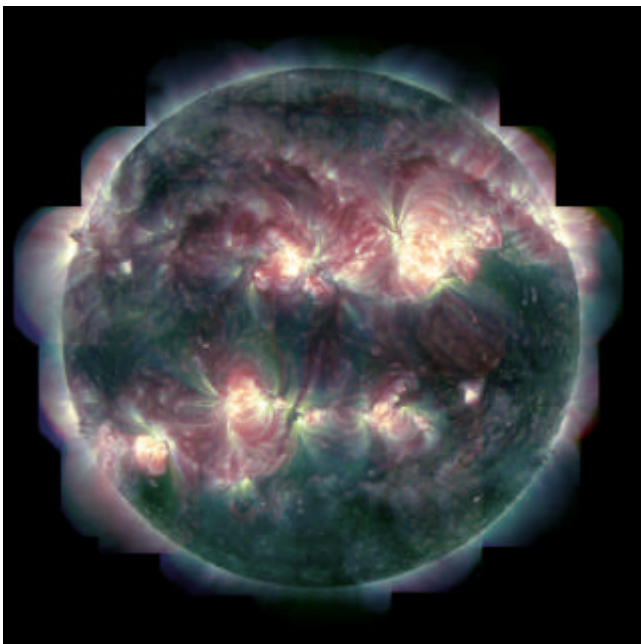


Figure 4. Complexities of solar structures as seen by the TRACE spacecraft (Courtesy, TRACE consortium).

spheric. The term active region refers to practically any region on the solar surface that cannot be identified as a coronal hole or a quiet region. Thus, as expected, this category includes all kinds of active regions, from the small and simple to the large and complex, from the very young ones that are still developing to the ones that are in the process of decay. Because of the large number of active regions and their diverse categories, observational results associated with their FIP bias have tended to be presented statistically rather than individually.

To derive the FIP bias variations, McKenzie and Feldman²⁴ studied the ratio of low-FIP Fe XVII to high-FIP Ne IX using the ratio Fe XVII 15.01 Å/Ne IX 13.45 Å. For these two ions the emissivity functions given by $G(T)$ overlap moderately well so that the Fe XVII/Ne IX line ratio is only weakly dependent on the temperature, which could in any case be monitored with the temperature-dependent Fe XVII 15.01 Å/Fe XVIII 14.2 Å line ratio. The extreme examples correspond to Fe/Ne abundance ratios of 0.27 and 1.12 respectively, a range of a factor of 4.1. Widing and Feldman²⁵ also studied the O/Ne and Mg/Ne abundance ratios in a small sample of active regions observed by Skylab. For three of the active regions, the FIP bias factor given by $(\text{Mg}/\text{Ne})/0.296$ reached values of 4.8, 5.4 and 5.9, significantly greater than the standard factor of 4 in the solar wind. This provides an additional illustration that when active regions are observed with sufficient spatial resolution, the measured FIP bias could significantly exceed a factor of 4. The abundance ratio of two low-FIP elements using the Fe XVIII 14.2 Å/Mg XI 9.17 Å intensity ratios provided the average Fe/Mg abundance ratio that McKenzie and Feldman derived was 0.80 in close agreement with a solar abundance ratio of 0.85 based on C I chondrites⁵.

Studying the FIP bias of the very high temperature regime in flares ($\sim 2 \times 10^7$ K) is not a straightforward task. This is because at such temperatures one sees primarily He-like and H-like lines of the low-FIP Fe and Ca, with no lines from high FIP ions for comparison. At somewhat lower temperatures, H-like lines of the high-FIP Ar are also expected. Unfortunately, thus far there are few flare spectra^{26,27} where statistically reliable comparisons between say H-like Ar-line intensities and He-like Ca-line intensities could be made. Thus for the most part the FIP bias determinations in the very high temperature plasmas were done using ratios between the Fe or Ca lines and the continuum, which in large part, depends on the H and He abundances. Many authors²⁸ studied these ratios and found FIP biases in flares to vary by factors of 4, values somewhat similar to those found in active regions.

Average FIP bias in coronal holes and quiet regions

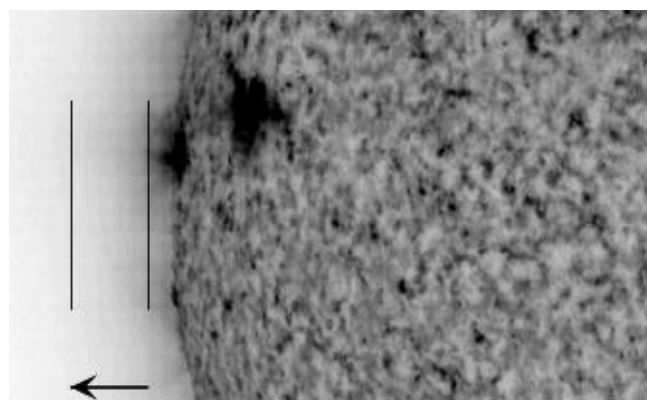
When reporting on the composition of coronal plasma, an important question to settle is the FIP-bias variation as a

function of height. In principle, to answer this question one needs to determine the FIP bias at a variety of limb heights, a tedious undertaking. In studying the spectra emitted by an equatorial quiet Sun streamer, Feldman *et al.*²⁹ found that the plasma occupying the streamer in the 1.05–1.5 R_⊙ height range is isothermal at a constant temperature of $\sim 1.4 \times 10^6$ K. Based on this finding, it was fairly straightforward for them to determine if elemental settling with height does exist. The fact that the intensities of the Ne VIII, Mg X, Si XI and Si XII lines decreased with height at the same rate, is consistent with the finding that the temperature does not vary with height. More importantly, the fact that the intensity ratios of the Ne VIII (high-FIP) and Mg X (low-FIP) lines and other low-FIP lines do not vary with height shows that the FIP bias also does not vary with height, at least, as far as elements with similar atomic weights are concerned. Feldman *et al.*³⁰ analysed the composition of the corona above the polar coronal hole in the same manner that they analysed the composition of the corona above the equatorial regions. They studied FIP bias as a function of temperature for low- and high-FIP lines emitted by the corona above a polar coronal hole. They found the FIP bias in the corona above the coronal hole to be very close to 1. It appears that the coronal plasma did not undergo any composition modification after emerging from under the photosphere.

The FIP bias rate of change in solar atmosphere regions

Among the most interesting issues associated with elemental abundances in the solar atmosphere regions is the rate of abundance change and the maximum value that such changes can reach. In considering the second issue, it is known that samples of the diffuse quiet corona and the large-scale averages of coronal plasmas sampled in the slow solar wind indicate maximum bias values of 4 or 5. On the other hand, in their survey of the Mg/Ne abun-

dance ratio in a variety of solar structures, Widing and Feldman¹³ observed a range of bias values greater than 4, including one that reached a FIP bias of 15 in an old open-field region. More recently, using the CDS instrument on SOHO, Young and Mason³¹ observed a FIP bias of 8.1 in a spiky structure lying at the edge of a newly emerged active region, which showed nearly photospheric abundances. The Mg/Ne abundance ratio was derived from the observed intensity ratio of Mg VI 349.2 Å to Ne VI 562.8 Å. Dwivedi *et al.*^{32,33} also derived a Mg/Ne abundance ratio from Mg VI/Ne VI line intensity ratios observations by SUMER spectrograph on 20 June 1996 above the active region NOAA 7974 at the solar east limb, as shown in Figure 5. In one active region located above the limb that was most likely a set of loop-like structures, FIP bias values of 8–16 were observed over a range of heights, with the variation probably reflecting the dominance of different loops. Mohan *et al.*^{34,35} investigated the Mg/Ne, S/Ar, Si/Ar and K/Ar abundance ratios as a function of position in the off-disk solar corona. The field of view composed of cold (6×10^5 K) plasma structures embedded in a hotter unstructured plasma at 1.8×10^6 K, as seen in the intensity maps obtained from Mg VI and S X lines are shown in Figure 6. The intensity, temperature and density maps of the cooler plasma inside the active region are shown in Figure 7 and their respective values in Figure 8. As we see in Figure 7, the variation of the Mg/Ne relative abundance is clearly correlated with the plasma structures. Some structures with strong Ne VI and Mg VI line emission indicate a normal Mg/Ne FIP bias between 1.6 to 3.2,



Raster direction

Figure 5. SUMER field-of-view superimposed to the EIT 304 channel observing chromospheric plasma.

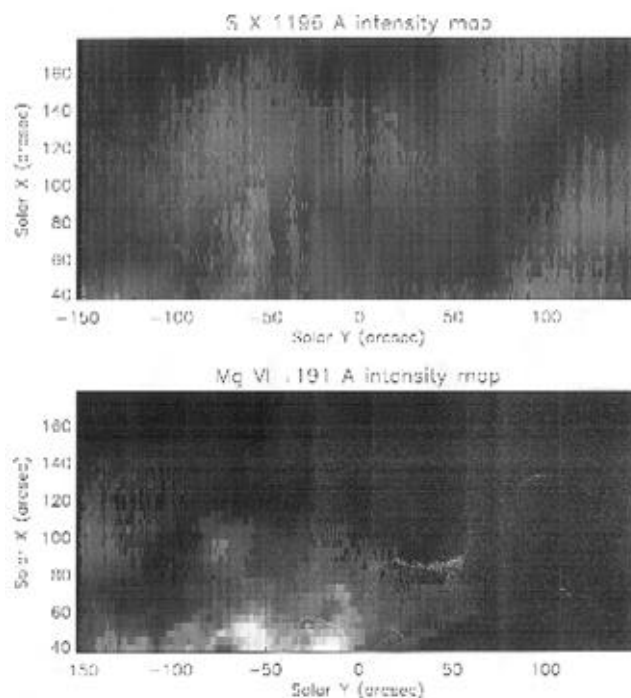


Figure 6. SUMER field-of-view. (Top) S X 1196 Å (active corona); (Bottom) Mg VI 1191 Å (cool structures).

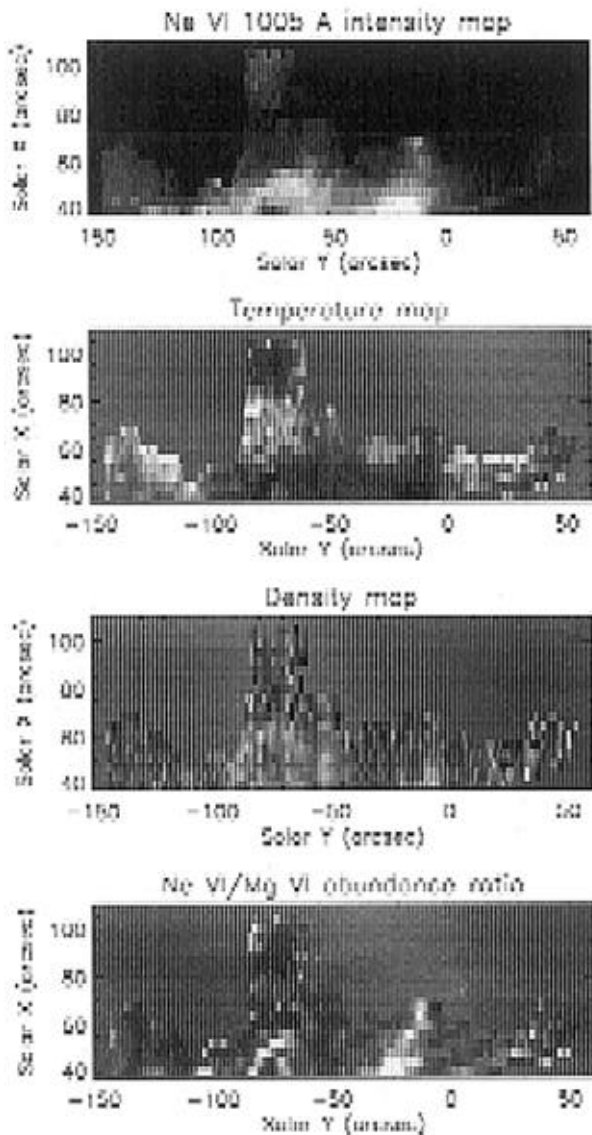


Figure 7. Diagnostic results in the active region structure. (From top) Ne VI 1005 Å intensity map of structures; Temperature map from Mg VII/Mg VI line ratio; Density map from the Mg VI line ratio; Ne VI/Mg VI line ratio yielding an estimate of the Ne/Mg abundance.

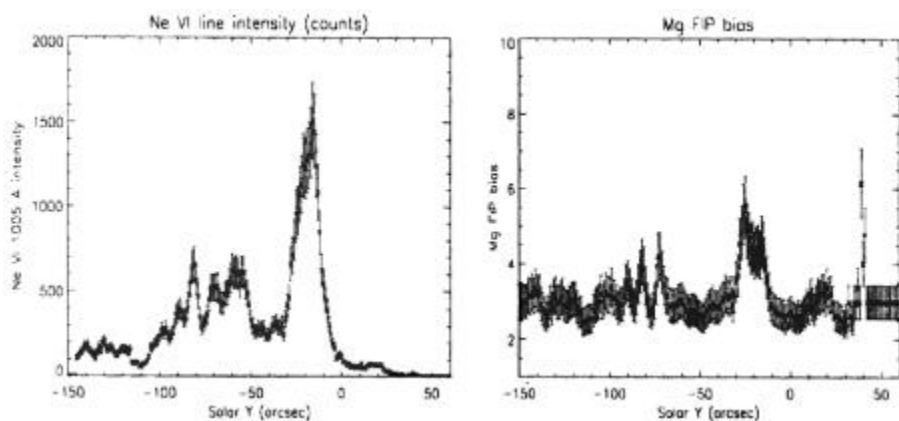


Figure 8. Cool plasma diagnostics (Left) Ne VI line intensity showing the presence of plasma structure; (Right) Mg/Ne FIP bias.

while in some other structures the Mg/Ne FIP bias ranges from 3.1 to 8.8. These values show that the plasma structuring has a strong effect on element abundances. An example is given in Figure 8, where the Ne VI intensity and FIP bias are shown.

Evidence of the FIP-bias to be FIP-dependent

The presence of the well-defined step function in the graph showing the FIP bias as a function of FIP in the quiet solar atmosphere suggests a simple relationship between the presence of an enrichment and the ionization conditions in the 5500 K photosphere. This relationship suggests that all elements already ionized in the photosphere (low-FIP) undergo an identical enrichment process, while those that stay neutral (high-FIP) remain unchanged. If this is indeed the case, then it may be reasonable to expect that in the very low-temperature photospheric regions (~ 3000 K), i.e. near sunspots, the FIP value that will discriminate between the low- and high-FIP elements will be lower than the typical 10 eV observed in quiet regions. In cases where the value that discriminates between low- and high-FIP values will be reduced say to $\text{FIP} \leq 7.0$ eV, the most abundant elements to be considered as low FIP would be K (FIP = 4.3 eV), Na (FIP = 5.1 eV), Al (FIP = 6.0 eV) and Ca (FIP = 6.1 eV). By contrast, under such conditions Mg (FIP = 7.6 eV), Si (8.1 eV) and Fe (FIP = 7.9 eV) will be expected to behave in the manner that high-FIP elements do.

In the pre-SOHO era, the Skylab spectroheliograph was the only space instrument with sufficiently high spatial resolution available for solar studies. The CDS and SUMER instruments on-board the SOHO spacecraft have the required spatial resolution properties (in addition to a separation between spatial and spectral resolution, where necessary) to detect such an effect. There are cases where the FIP bias of the very low FIP elements (FIP ~ 6 eV) appears to be higher by about a factor of 2 than the FIP bias for elements having a FIP ~ 8 eV. This may suggest that a FIP

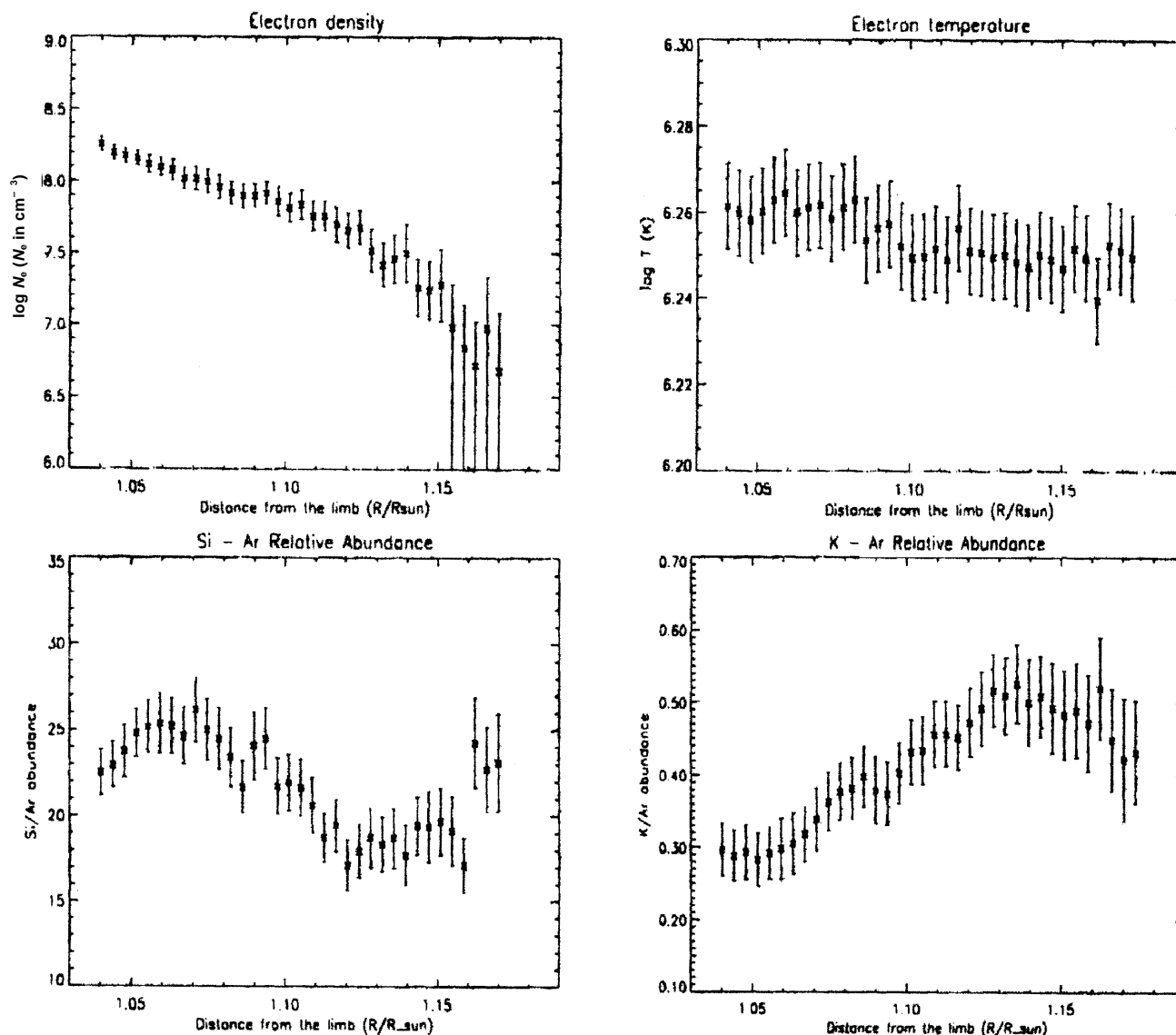


Figure 9. Active corona diagnostics. (Top left) $\log N_e$ versus height; (Top right) $\log T$ versus height; (Bottom left) Si/Ar abundance versus height; (Bottom right) K/Ar abundance versus height.

bias vs FIP dependency exists, but it is by no means a definitive confirmation of such an effect.

Dwivedi *et al.*³⁶ re-analysed the low-FIP/high-FIP pairs such as S/Ar, Si/Ar and K/Ar as a function of height, as shown in Figure 9. The coronal relative abundance of S/Ar stays almost at its photospheric value; Si/Ar shows a FIP bias of 2 to 3; K/Ar shows a FIP bias increasing with height from 6.4 to 14. The FIP bias for the very low FIP elements such as K could be higher than for the normal low-FIP elements such as Mg, Si and Fe, so that the FIP effect for the low-FIP elements could be dependent on the FIP itself. The evident height dependence of the K FIP bias is a new observational fact, whose magnitude is larger than the combined experimental and theoretical uncertainties.

Concluding remarks

The main result from the survey of the FIP bias in solar observations is how closely the FIP effect is associated with the loop-like structures which manage to confine plasmas for extended times. Clearly no FIP effect is present in coronal holes where loop-like structures that may confine the coronal plasma do not exist. Similarly, in the 3×10^4 K– 6×10^5 K plasma regions where loop-like structures are short-lived, the FIP effect is small. From a SUMER/SOHO raster study of activity above the limb Dwivedi *et al.*^{32,33} concluded that FIP fractionation strongly depends on plasma structures. The analysis of the diffuse corona seems to suggest that in off-limb active region plasma the FIP bias inside the class of low-FIP elements is dependent on

the FIP value, being higher for the very low FIP element K^{34-36} . Also, some dependence of the FIP bias with height is suggested. The FIP bias versus FIP problem is still open and further work is required.

1. Russell, H. N., On the composition of the sun's atmosphere. *Astrophys. J.*, 1929, **70**, 11–82.
2. Grevesse, N. and Sauval, A. J., Abundances of the elements in the Sun. In *Origin of Elements in the Solar System: Implications of Post-1957 Observations* (ed. Manuel, O.), Kluwer Academic/Plenum Publishers, 2000, pp. 261–277.
3. Unsöld, A., Quantitative analyse der sonnenatmosphäre. *Z. Astrophys.*, 1948, **24**, 306–326.
4. Grevesse, N. and Sauval, A. J., Standard solar composition. *Space Sci. Rev.*, 1998, **85**, 161–174.
5. Anders, E. and Grevesse, N., Abundances of the elements: Meteoritic and solar. *Geochim. Cosmochim. Acta*, 1989, **53**, 197–294.
6. Hovestadt, D., Nuclear composition of solar cosmic rays. In *Solar Wind III* (ed. Russel, C. T.), Univ. California, Los Angeles, 1974, p. 2.
7. Geiss, J., Processes affecting abundances in the solar wind. *Space Sci. Rev.*, 1982, **33**, 201–217.
8. Breneman, H. H. and Stone, E. C., Solar coronal and photospheric abundances from solar energetic particle measurements. *Astrophys. J. Lett.*, 1985, **299**, L57–L61.
9. Pottasch, S. R., The lower solar corona: Interpretation of the ultraviolet spectrum. *Astrophys. J.*, 1963, **137**, 945–966.
10. Pottasch, S. R., On the interpretation of the solar ultraviolet emission line spectrum. *Space Sci. Rev.*, 1964, **3**, 816–855.
11. Goldberg, L., Müller, E. and Aller L. H., The abundances of the elements in the solar atmosphere. *Astrophys. J. Suppl.*, 1960, **5**, 1–137.
12. Meyer, J. P., Solar–stellar outer atmospheres and energetic particles, and galactic cosmic rays. *Astrophys. J. Suppl.*, 1985, **57**, 173–204.
13. Widing, K. G. and Feldman, U., Elemental abundances and their variations in the upper solar atmosphere. In *Solar Wind Seven* (eds Marsch, E. and Schwenn, R.), Pergamon Press, 1992, pp. 405–410.
14. Seaton, M. J., The spectrum of the solar corona. *Planet. Space Sci.*, 1964, **12**, 55–74.
15. Dwivedi, B. N., Mohan, A. and Thomas, R. J., Spectral diagnostics of the active region observed by the Solar EUV Rocket Telescope and Spectrograph (SERTS). *Solar Phys.*, 1998, **180**, 157–178.
16. Arnaud, M. and Rothenflug, R., An updated evaluation of recombination and ionization rates. *Astron. Astrophys. Suppl.*, 1985, **60**, 425–457.
17. Mazzotta, P., Mazzitelli, G., Colafrancesco, S. and Vittorio, N., Ionization balance for optically thin plasmas: Rate coefficients for all atoms and ions of the elements H to Ni. *Astron. Astrophys. Suppl.*, 1998, **133**, 403–409.
18. Dere, K. P., Landi, E., Mason, H. E., Monsignori-Fossi, B. C. and Young, P. R., CHIANTI – an atomic database for emission lines. *Astron. Astrophys. Suppl.*, 1997, **125**, 149–173.
19. Landi, E. *et al.*, CHIANTI – an atomic database for emission lines. III. Continuum radiation and extension of the ion database. *Astron. Astrophys. Suppl.*, 1999, **135**, 339–346.
20. Gabriel, A. H. *et al.*, Spacelab 2 measurement of the solar helium abundance. *Adv. Space Res.*, 1995, **15**, 63–67.
21. Feldman, U., FIP effect in the solar upper atmosphere: Spectroscopic results. *Space Sci. Rev.*, 1998, **85**, 227–240.
22. Laming J. M. and Feldman, U., The solar helium abundance in the outer corona determined from observations with SUMER/SOHO. *Astrophys. J.*, 2001, **546**, 552–558.
23. Sheeley Jr., N. R., A volcanic origin for high-FIP material in the solar atmosphere. *Astrophys. J.*, 1995, **440**, 884–887.
24. McKenzie, D. L. and Feldman, U., Variations in the relative elemental abundances of oxygen, neon, magnesium, and iron in high-temperature solar active-region and flare plasmas. *Astrophys. J.*, 1992, **389**, 764–776.
25. Widing K. G. and Feldman, U., Abundance ratios of oxygen, neon, and magnesium in solar active regions and flares: The FIP effect. *Astrophys. J.*, 1995, **442**, 446–450.
26. Doschek, G. A., Feldman, U. and Seely, J. F., Element abundances from solar flare spectra. *Mon. Not. R. Astron. Soc.*, 1985, **217**, 317–326.
27. Doschek, G. A. and Seely, J. F., The Ar/Ca abundance ratio in solar flares. *Astrophys. J.*, 1990, **348**, 341–345.
28. Sterling, A. C., Doschek, G. A. and Feldman, U., On the absolute abundance of calcium in solar flares. *Astrophys. J.*, 1993, **404**, 394–402.
29. Feldman, U., Widing, K. G. and Warren H. P., Morphology of the quiet solar atmosphere in the $4 \times 10^4 < Te < 1.4 \times 10^6$ K temperature regime. *Astrophys. J.*, 1999, **522**, 1133–1147.
30. Feldman, U., Schühle, U., Widing, K. G. and Laming, J. M., Coronal composition above the solar equator and the north pole as determined from spectra acquired by the SUMER instrument on SOHO. *Astrophys. J.*, 1998, **505**, 999–1006.
31. Young, P. R. and Mason, H. E., The Mg/Ne abundance ratio in a recently emerged flux region observed by CDS. *Solar Phys.*, 1997, **175**, 523–539.
32. Dwivedi, B. N., Curdt, W. and Wilhelm, K., Analysis of EUV off-limb spectra obtained with SUMER/SOHO: Ne VI/Mg VI emission lines. *Astrophys. J.*, 1999, **517**, 516–525.
33. Dwivedi, B. N., Curdt, W. and Wilhelm, K., The off-limb behaviour of the FIP effect in the solar atmosphere observed by SUMER on SOHO. European Space Agency (ESA), 1999, **SP-446**, 293–298.
34. Mohan, A., Dwivedi, B. N. and Landi, E., Electron density and temperature measurements, and abundance anomalies in the solar atmosphere. *J. Astrophys. Astron.*, 2000, **21**, 407–411.
35. Mohan, A., Landi, E. and Dwivedi, B. N., FIP effect measurements in the off-limb corona observed by SUMER on SOHO. *Astron. Astrophys.*, 2000, **364**, 835–844.
36. Dwivedi, B. N., Mohan, A. and Landi, E., FIP effect and the FIP-dependent bias in the solar atmosphere. In *ASP Conference Series, S219: Stars as Suns: Activity, evolution and planets* (eds Dupree, A. K. and Benz, A. D.), 2003, in press.

ACKNOWLEDGEMENTS. This work is supported by SERC/DST, New Delhi under its Fast Track Scheme. We thank the referee for helpful comments.

Received 10 October 2003; revised accepted 13 January 2004